Efficiency of pecan shells and sawdust biochar on Pb and Cu adsorption

K. Komnitsas[a,*], D. Zaharaki[a], G. Bartzas[b], G. Kaliakatsou[a], A. Kritikaki[a]

[a]*School of Mineral Resources Engineering, Technical University Crete, Chania, Crete 73100, Greece, Tel. +30 28210 37686;*
Fax: +30 28210 69554; email: komni@mred.tuc.gr (K. Komnitsas)
[b]*School of Mining and Metallurgical Engineering, National Technical University of Athens, Zografos Campus, Athens 15780,*
Greece

ABSTRACT

In the present study, two different by-products, pecan shells, and sawdust obtained from the region of Chania, Crete, Greece, were subjected to slow pyrolysis over a temperature range of 250–550°C, for the production of biochar. The quality of the produced biochars was assessed by evaluating their main properties, namely pyrolysis yield, pH, volatile matter and char content, surface area, and C, H, S, N content. Thermogravimetric analysis, Fourier transform infrared spectroscopy, X-ray diffraction, and scanning electron microscopy were used for the identification of the morphology and structure of the produced biochars. The potential of selected pecan shells and sawdust biochars to adsorb Pb and Cu from synthetic solutions was also assessed.

Keywords: Biochar; Pyrolysis; Morphology; Structure; Adsorption

1. Introduction

Biochar is a carbon rich, solid, and porous material produced after heating of biomass at moderate temperature under limited or oxygen free atmosphere. The thermochemical processes used for its production involve slow or fast pyrolysis, conventional or flash carbonization, and gasification. Slow pyrolysis, which involves thermal treatment of biomass by slow heating at low to medium temperatures (350–650°C) in a low oxygen atmosphere, has the advantage of retaining almost half of the feedstock carbon in stable biochar [1]. Other products that may result from pyrolysis of biomass include syngas or pyrolysis gas, which can be used as fuel source, as well as bio-oil which can be used as substitute to fossil fuels [2,3].

The chemical and physical properties of biochars are greatly affected both by the composition of the feedstock as well as by the process followed. The most important characteristic of biochar is its porous structure which plays a significant role in its use as soil amendment by increasing its surface area and retention of soil water. Moreover, biochar is a very promising alternative for carbon sequestration, mitigation of global warming, renewable energy generation, and adsorbent for the removal of organic and inorganic contaminants from wastewaters, soils, and hazardous wastes [4–6].

Biochar exhibits increased chemical and biological stability, and when applied to soils, due to its noticeable adsorption potential, it may improve soil fertility, acting as slow release fertilizer, and inhibit mobilization of organic and inorganic contaminants toward

*Corresponding author.

deeper soil horizons, thus preventing contamination of groundwater [7–9].

Biochar can be produced in every country using various raw materials including energy crops (e.g. corn, cereals, wood pellets, and oilseed rape), agricultural wastes (e.g. manure, wheat straw, rice husk, waste wood, pistachio, peanut, and hazelnut shells) and other wastes including sewage sludge [10–13].

In the present paper, biochars produced after slow pyrolysis of pecan shells and sawdust have been characterized by evaluating the main properties such as pyrolysis yield, pH, volatile matter, char content, surface area, and C, H, S, N content. Analytical techniques, namely TG, FTIR, XRD, and SEM have been used for the identification of their morphology and structure. The potential of selected pecan shells and sawdust biochars to adsorb Pb and Cu from synthetic solutions was also assessed.

2. Materials and methods

In the present study, two different raw materials, pecan shells (Pe) obtained from trees cultivated in the region of Chania, Crete, Greece, and sawdust (Sd) obtained from a local carpentry, were subjected to slow pyrolysis for the production of biochar.

Pyrolysis of small quantities, e.g. 30 g of each raw material, was carried out in a modified laboratory furnace, N-8L SELECTA, at temperatures varying between 250 and 550°C, using porcelain capsules. Nitrogen was fed in the oven at a rate of 100 mL min^{-1} for 60 min to remove air. The heating rate was maintained at 10°C min^{-1} and the retention time of the feedstock in each temperature was 60 min.

Pyrolysis yield (y_P) was determined for all biochars produced from the % weight loss after heating. In raw materials and biochars, pH and oxidation–reduction potential were measured using a solid:liquid ratio of 1:10 with a Hanna 211 pH/Eh meter while electrical conductivity (EC) with a Hanna EC215 conductivity meter. Surface area was measured using NOVA surface area analyzer (Quantachrome instruments). The elemental C, H, S, and N analysis was carried out in a flash 2000 elemental analyzer thermo scientific calibrated using BBOT standards (2,5-Bis(5-tert-butyl-2-benzo-oxazol-2-yl)thiophene) containing carbon; the oxygen content was subsequently calculated as the difference.

Biochars were subjected to thermogravimetric analysis using a differential thermogravimetric analyzer Diamond DTA-TG of Perkin Elmer (temperature measurement precision of ±2°C, microbalance sensitivity <5 μg). The rate and % weight loss for each sample were determined continuously as a function of time or temperature, under dynamic conditions, in the range of 40–850°C. The experiments were carried out at atmospheric pressure, under nitrogen atmosphere, with a flow rate of 100 mL min^{-1} and a heating rate of 10°C min^{-1}. Volatile matter (VM) and char content were also determined. All experiments were carried out in duplicate.

Fourier transform infrared spectroscopy (FTIR) analysis of samples was carried out using a Perkin Elmer spectrum 1000 (USA); for the production of the pellets, each sample was mixed with KBr at a ratio 1:100 w/w. X-ray diffraction (XRD) analysis was performed using a Bruker D8 advance diffractometer with a Cu tube and a scanning range from 3° to 70° 2θ with a step 0.03° and 4 s/step measuring time. Qualitative analysis was carried out using the diffracplus software (Bruker AXS) and the PDF database. Scanning electron microscopy (SEM) analysis was carried out with a JEOL 6380LV SEM equipped with an EDS INCA microanalysis system with low vacuum, pressure 30 Pa, voltage 20 kV, and 10–12 mm sample distance (working distance) from the detector.

Adsorption experiments were carried out using pecan and saw dust biochars prepared after pyrolysis at 350°C for 60 min (Pe350 and Sd350, respectively). Two solutions of 100 mg L^{-1} Pb and 100 mg L^{-1} Cu were prepared by dissolving the required quantities of Pb(NO$_3$)$_2$ and Cu(NO$_3$)$_2$·3H$_2$O, respectively, in distilled water. For each solution the adsorbent concentrations used was 5 g L^{-1}. After equilibrium at 24 h, desorption experiments were carried out over a period of 24 h using 0.1 N HNO$_3$ and 0.1 N HCl. Adsorption and desorption experiments were successively carried out until equilibrium was reached. Agitation took place on a Vibromatic rocking mixer at 350 rpm and room temperature. Pb and Cu concentrations were determined using a Perkin Elmer Analyst 100 flame atomic absorption spectrophotometer. All tests were carried out in triplicate.

3. Results and discussion

3.1. Characterization of raw materials and biochars

Table 1 shows the characterization of pecan shells (Pe), sawdust (Sd), and the biochars produced at 250, 350, 450, and 550°C (Pe250, Pe350, Pe450, Pe550 and Sd250, Sd350, Sd450, Sd550, respectively).

The quality of biochars produced is quite similar for both by-products used. As temperature increases from 250 to 550°C, the pyrolysis yield decreases from 74.2 to 21.7% for pecan shells while a more noticeable decrease from 77 to 7.8% is shown for sawdust. For both Pe and Sd, the low pyrolysis yield obtained at

Table 1
Characterization of Pe, Sd, and the biochars Pe250–Pe550, and Sd250–Sd550

	Pe	Pe250	Pe350	Pe450	Pe550	Sd	Sd250	Sd350	Sd450	Sd550
y_P, %	–	74.2	44.5	30.3	21.7	–	77.0	30.6	13.8	7.8
pH	5.8	4.9	4.9	6.3	6.8	5.7	4.4	3.8	5.0	6.6
EC, mS cm^{-1}	0.32	0.28	0.22	0.66	0.80	0.38	0.17	0.20	0.22	0.42
VM, %	71.3	56.2	40.9	37.4	23.0	89.6	67.2	42.9	38.5	35.7
Char, %	28.7	43.8	59.1	62.6	77.0	10.4	32.8	57.13	61.5	64.2
Surface area, m^2 g^{-1}	–	3.2	3.2	165.4	298.7	–	2.5	2.6	66.8	84.6
% C	47.4	54.6	65.6	74.8	76.4	46.7	52.3	63.2	66.8	68.0
% H	5.39	4.32	3.01	2.08	1.94	5.81	3.54	2.09	1.88	1.51
% N	0.63	0.61	0.60	0.57	0.55	0.51	0.46	0.32	0.19	0.14
% O	46.58	40.47	30.79	22.55	21.11	46.98	43.7	34.39	31.13	30.35

temperatures higher than 350°C is due to the condensation of aliphatic compounds and loss of CH_4, H_2, and CO. The pyrolysis yield of several other biomass feedstocks, namely oak wood, pine wood, olive husk, corncob, and straw is in the same range [3,14].

pH drops during pyrolysis up to 350°C and increases when higher temperatures (up to 550°C) are used. Thus, biochar produced at low temperatures may be used as amendment in alkaline soils, while biochar produced at higher temperatures may buffer pH in slightly acidic soils. A similar trend is shown for EC. In other studies, pH values up to 8.6 have been reported for biochars produced after pyrolysis of other agricultural wastes at 500°C [15].

Increased pyrolysis temperature (from 250 to 550°C) results in substantial decrease in the volatile matter (VM) content (from 71.3 to 23% for Pe and 89.6 to 35.7% for Sd). At higher temperatures, aliphatic-C structures are affected thus enhancing the potential of biochar as soil amendment. Increase in pyrolysis temperature results also in increased char content reaching 77 and 64.2% at 550°C, for Pe and Sd, respectively.

High surface area values are shown when biochars are produced at temperatures higher than 450°C reaching 298.7 and 84.6 m^2 g^{-1}, respectively, for Pe550 and Sd550. Similar results have been also reported in other studies [16,17].

For both Pe and Sd biochars, increase in pyrolysis temperature from 250 to 550°C results in increased total carbon content and decreased hydrogen, nitrogen, and oxygen content. Comparable results are reported by Gaskin et al. [18], indicating that the carbon content of biochars produced from pine chips, peanut hulls, and switchgrass at 400–500°C was close to 80%.

3.2. TG and DTG analysis

Fig. 1 shows the TG (weight loss) and DTG (weight loss rate) curves versus temperature, for Pe and biochars Pe350 and Pe550 (Fig. 1(a) and (b), respectively) as well as for Sd and biochars Sd350 and Sd550 (Fig. 1(c) and (d), respectively). The noise shown in some parts of the curves is due to instrumental difficulties.

The total calculated weight loss decreases when pyrolysis temperature increases and reaches 73, 44, and 23% for Pe, Pe350, and Pe550, and 89, 49, and 43% for Sd, Sd350, and Sd550, respectively. A sharp weight loss is shown for Pe and Sd, while the weight loss is smooth for biochars produced at 550°C.

DTG curves in Fig. 1(b) and (d) shows that the major weight loss was initiated at around 300°C as confirmed by the respective TG curves (Fig. 1(a) and (c)). In the DTG curve of Pe (Fig. 1(b) two distinct peaks, typical for lignocellulose materials, are clearly shown. The first peak at around 300°C represents the decomposition of hemicellulose which decomposes at 150–350°C. The second peak at around 350°C, which is also shown in the DTG curve of Sd (Fig. 1(d), corresponds to the decomposition of cellulose which usually takes place in a relatively narrow temperature range of 275–350°C. The presence of cellulose is also confirmed by the XRD analysis, as discussed below. The gradual decomposition of lignin over a wider temperature range (usually at 275–500°C) is represented by the flat section shown in Fig. 1(b) and (d) [19–21].

3.3. FTIR analysis

Fig. 2 shows the FTIR spectra of pecan shells (Pe), sawdust (Sd), and selected biochars (Pe350, Pe550, Sd350, Sd550), while the FTIR spectra band assignments are presented in Table 2. Both Sd and Pe spectra are characteristic of a generic oxygenated hydrocarbon due to its cellulose content. As pyrolysis temperature increases FTIR spectra show a loss of chemical diversity compared to the raw materials (Pe and Sd) and major bands disappear.
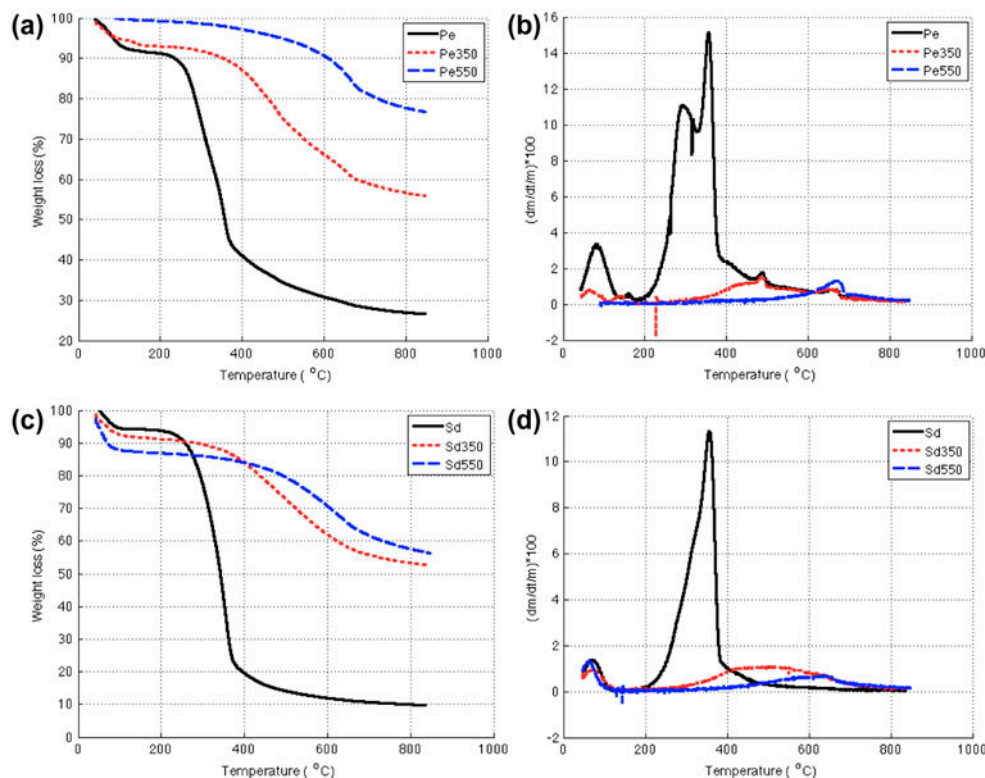
Fig. 1. TG and DTG curves versus temperature, for Pe and biochars Pe350, Pe550 ((a) and (b)) and Sd and biochars Sd350, Sd550 ((c) and (d)).
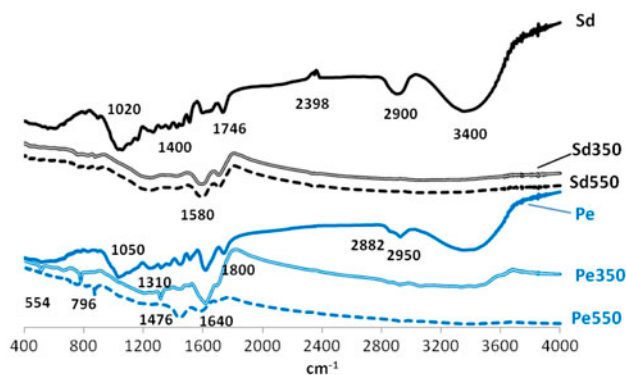

Fig. 2. FTIR spectra of Pe and biochars Pe350 and Pe550, as well as Sd and biochars Sd350 and Sd550.

The broad bands seen for raw materials, Pe and Sd, at around 3,430 cm^{-1} indicate the presence of free and intermolecular bonded hydroxyl group (−OH) stretching. In biochars, produced under pyrolysis at 350 and 550°C these bands have disappeared, indicating the absence of hydroxyl content and increase in hydrophobicity of biochars. The peaks at 2,950, 2,900, and 2,882 cm^{-1}, seen only in Pe and Sd, are due to aliphatic C–H deforming vibration. The small band at

2,398 cm^{-1} is due to the presence of atmospheric carbon dioxide.

The band at around 1,800 cm^{-1} seen in all samples, is assigned to ν(C=O) vibration in carbonyl group or the presence of carboxylic bonds. The intensity of these bands decreases slightly at higher temperatures due to the decomposition of carbonate compounds. The bands at around 1,600 cm^{-1} are due to the presence of aromatic C=O ring stretching (likely –COOH) or C=C stretching of aromatic groups in lignin implying the presence of residual lignin after decomposition. These bands are also strong in the spectra of biochars. The ratio of these peaks has been also found to reflect the degree of charring of cellulose.

The characteristic group of peaks which appears at 1,400–1,500 cm^{-1} only in raw materials Pe and Sd and disappear in all biochars is attributed to C6 ring modes. The intense bands occurring at 1,020 and 1,050 cm^{-1}, for Sd and Pe, respectively, are characteristic of a C–C−O or C–O−C asymmetric stretch or due to aliphatic ether, alcohol C–O or aromatic stretching, O–H deformation vibrations or b-glycosidic bonds in cellulose and hemicelluloses. These peaks disappear in all biochars indicating the decomposition of hemicellulose and cellulose.

Table 2
FTIR spectra band assignments corresponding to Fig. 2

Band number, cm^{-1}	Assignment	Refs.
3,400	Hydroxyl group (−OH) stretching	[22,23]
2,950, 2,900, 2,882	Aliphatic C–H deforming vibration	[17,24]
2,398	Atmospheric carbon dioxide	[25]
1,800, 1,746	ν(C=O) vibration in carbonyl group or presence of carboxylic bonds	[26,27]
1,640, 1,580	Aromatic C=O ring stretching (likely –COOH) or C=C stretching of aromatic groups in lignin	[28–31]
1,500–1,400	C6 ring modes	[14,32,33]
1,310	δ(C=H) vibration in alkanes and alkyl groups	[32]
1,050, 1,020	Aliphatic ether, alcohol C–O or aromatic stretching peak, O–H deformation vibrations, b-glycosidic bond in cellulose and hemicellulose	[14,31]
796	C–H stretching vibrations	[24]
554	−OH out of plane bending modes	[17]

Biochar Pe350 shows also three small peaks: at 1,310 cm^{-1} due to δ(C=H) vibration in alkanes and alkyl groups, at 796 cm^{-1} attributed to aromatic and heteroaromatic compounds confirmed by C–H stretching vibrations and also at 554 cm^{-1} due to −OH out of plane bending modes.

3.4. XRD analysis

The XRD pattern of pecan shells (Pe) and biochars produced by pyrolysis of pecan shells at 350 (Pe350) and 550°C (Pe550), are shown in Fig. 3. The XRD pattern of sawdust (Sd) and biochars Sd350 and Sd550, are presented in Fig. 4. In both raw materials (Pe and Sd), the characteristic amorphous peaks of cellulose, which is one of the important structural components of the primary cell wall of green plants, are detected. However, after pyrolysis these peaks are quite lower. The XRD patterns of Pe350 and Pe550 as well as Sd350 and Sd550 are quite similar and are characterized by the elevated background between 16° and 26° 2-theta, due to the presence of organic matter [27].

The peaks of residual inorganic phases, calcite, quartz, and whewellite in biochars, are more easily detected by XRD as a result of decomposition of organic phases in temperatures higher than 350°C. Their presence is due to impurities, such as atmospheric deposition of dust which may be present on trees as also reported elsewhere [34,35].

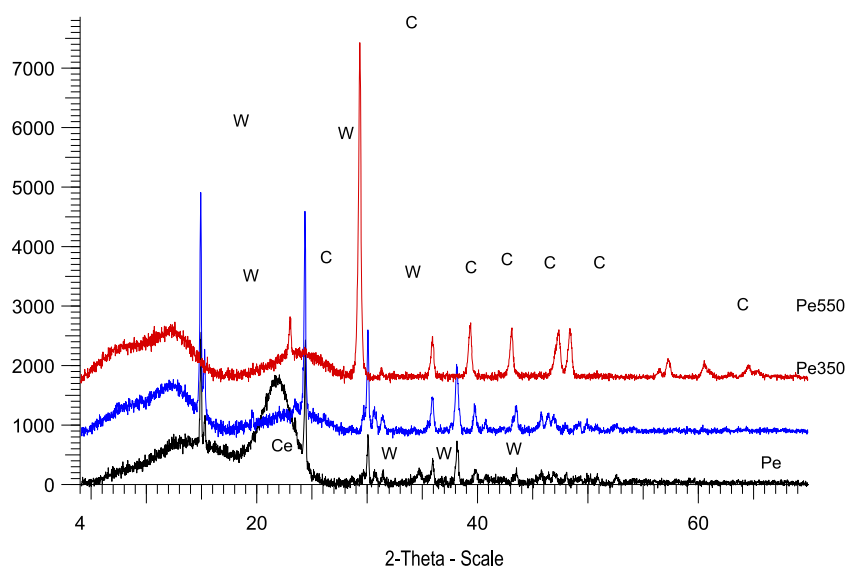Fig. 3. XRD pattern of pecan shells (Pe) and biochars produced by pyrolysis of pecan shells at 350 (Pe350) and 550°C (Pe550) (Ce: cellulose (C$_6$H$_{10}$O$_5$)$_n$, C: calcite CaCO$_3$, W: whewellite CaC$_2$O$_4$·H$_2$O).
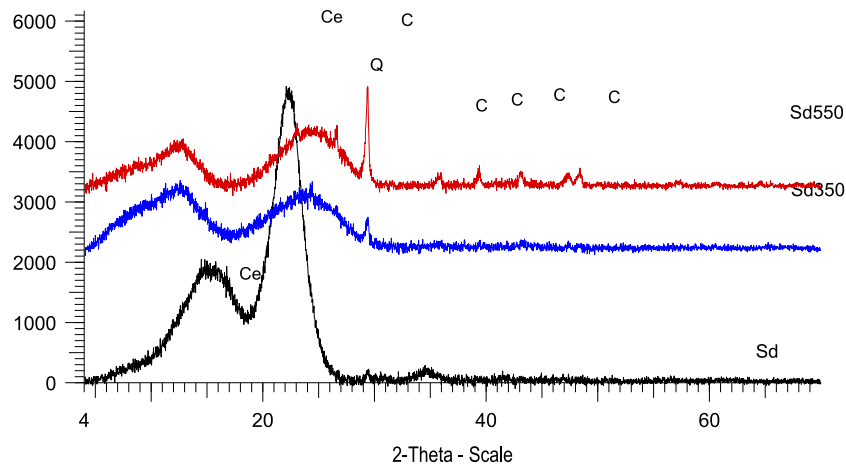
Fig. 4. XRD patterns of sawdust (Sd) and biochars produced by pyrolysis of sawdust at 350 (Sd350) and 550°C (Sd550) (Ce: cellulose $(C_6H_{10}O_5)_n$, C: calcite $CaCO_3$, Q: quartz SiO_2).

3.5. SEM analysis

In Figs. 5 and 6, SEM backscattered electron images (BSI) of Pe and biochars Pe350 and Pe550 as well as of Sd and biochars Sd350 and Sd550 are shown, respectively. It is seen from Fig. 5 that the matrix of raw Pe is quite homogeneous. When Pe is pyrolized for the production of biochar at 350°C (Pe350) or 550°C (Pe550) a microporous structure is formed, due to the release of volatiles, with particle size varying between 7 and 18 µm. Increase in pyrolysis temperature from 350 to 550°C also results in increased pore diameter and the development of new pores.

According to Fig. 6, the fibrous structure of sawdust (Sd) is slightly altered when pyrolysis takes place at 350°C (Sd350) or 550°C (Sd550). The increase in pyrolysis temperature from 350 to 550°C also increases pore diameter from 9–16 µm (micropores) to 21–48 µm (mesopores), respectively, as a result of the continuous

release of other high-molecular-weight volatiles. It is evident that when the pyrolysis temperature is increased from 350 to 500°C, very fine and oriented cellular mesopores with sharp and curvy edges are formed, suggesting clear development of pore structure.

It is reported by Gray et al. [30] that as temperature increases porosity increases as well due to the transformation of aliphatic C structures to aromatic C structures. The formation of new and well structured pores may contribute to the use of biochar as soil amendment as it can provide habitats for symbiotic micro-organisms [36].

The EDS analysis (not shown) carried out on the surface of samples reveals only the presence of impurities such as Al due to the use of ultra-fine corundum powder for polishing of the samples during preparation for SEM analysis, as well as Ca due to the presence of dust during raw material collection. These
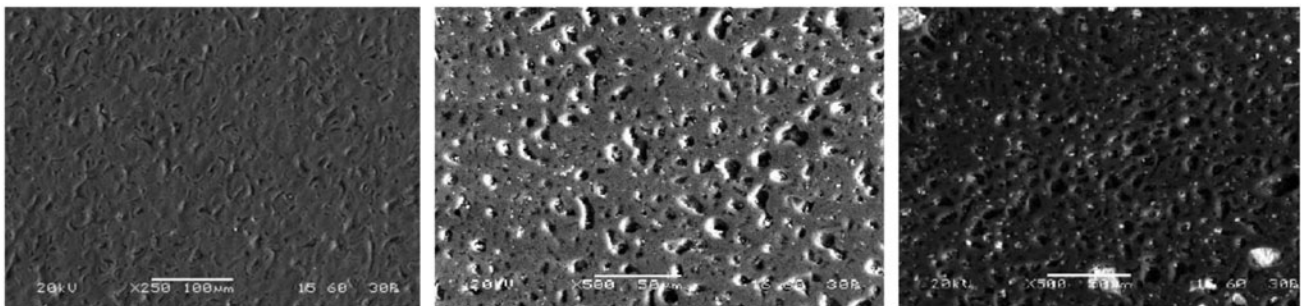

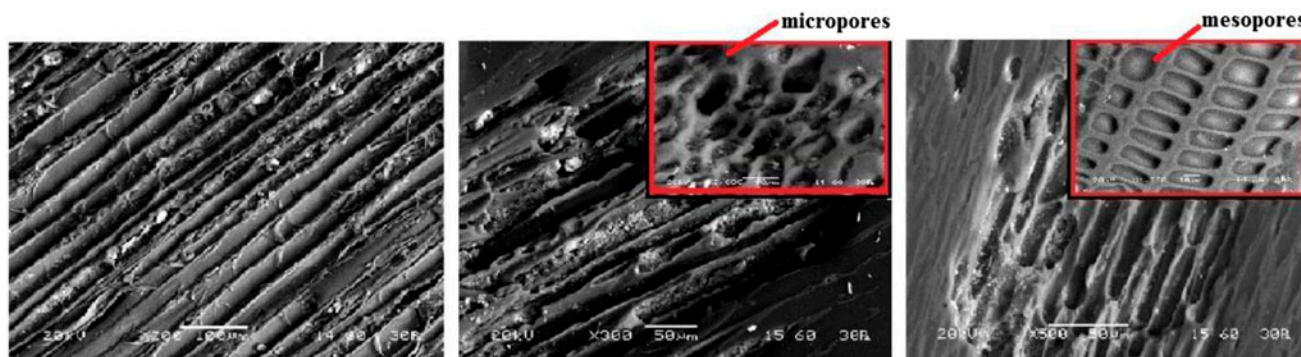Fig. 5. SEM-BSI images of the Pe (×250), Pe350 (×500), and Pe550 (×500) structures (left to right).

Fig. 6. SEM-BSI images of the Sd (×200), Sd350 (×300 and ×2,000), and Sd550 (×500 and ×1,000) structures (left to right).

findings are also confirmed by the XRD patterns discussed previously.

3.6. Pb and Cu adsorption potential of biochars

Fig. 7 shows the % Pb and Cu adsorption of biochars Pe350 and Sd350 when various adsorbent concentrations (0.1, 0.5, 1 and 5 g L^{-1}) are used in solutions containing 100 mg L^{-1} Pb or Cu. From Fig. 7 it can be deduced that for both biochars, Pb is adsorbed more efficiently compared to Cu. The Sd350 biochar shows

better adsorption behavior for both Pb and Cu, compared to Pe350 biochar.

For both heavy metal ions and biochars, the highest % adsorption is shown when the highest adsorbent concentration of 5 g L^{-1} is used. The % adsorption of heavy metals decreases with gradual decrease in the adsorbent concentration from 5 to 0.1 g L^{-1}. According to Fig. 7(a) for 5 g L^{-1} biochar Pe350, the highest % adsorption of Pb (95%) is obtained after 6 h, while the highest % adsorption of Cu is 14% (Fig. 7(c). Regarding Sd350, the highest %
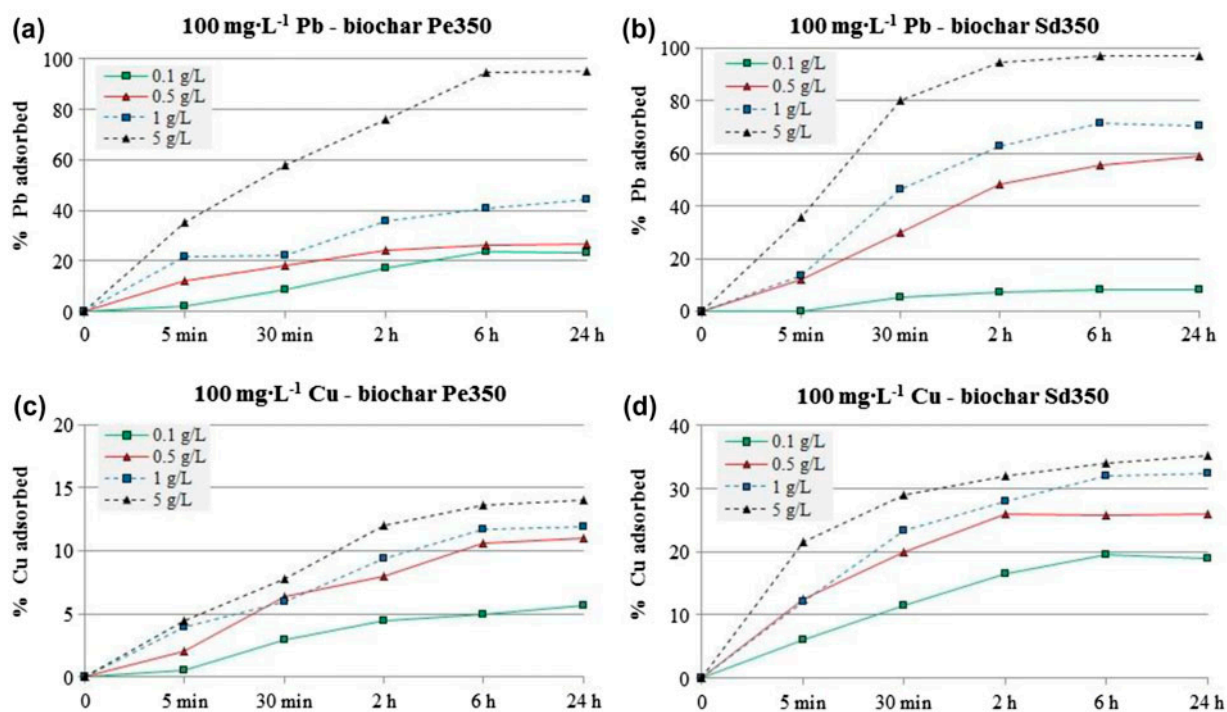

Fig. 7. % Pb and Cu adsorption of biochars Pe350 and Sd350 when various adsorbent concentrations (0.1, 0.5, 1, and 5 g L^{-1}) are used in solutions containing 100 mg L^{-1} Pb ((a) and (b)) or 100 mg L^{-1} Cu ((c) and (d)).

Table 3
Pb adsorption and desorption efficiency of biochars Pe350 and Sd350

	Cycle 1			Cycle 2			Cycle 3			Cycle 4	
	Adsorption Pb adsorbed mg g^{-1}	%	Desorption Pb desorbed %	Adsorption Pb adsorbed mg g^{-1}	%	Desorption Pb desorbed %	Adsorption Pb adsorbed mg g^{-1}	%	Desorption Pb desorbed %	Adsorption Pb adsorbed mg g^{-1}	%
Pe350*	17.9	95.2	86.6	11.2	60.3	53.2	7.1	37.2	28.3	4.6	24.2
Pe350**	17.7	94.1	65.0	9.8	51.6	35.6	5.2	25.4	11.3	4.1	21.3
Sd350*	18.3	97.3	94.0	17.6	94.7	84.7	12.3	64.8	56.7	7.6	39.8
Sd350**	18.2	96.6	90.7	17.5	94.2	79.7	10.3	55.2	42.5	6.4	31.7

*Desorption with HCl.
**Desorption with HNO$_3$.

adsorption of Pb and Cu are 97 and 35% after 6 h (Fig. 7(b) and (d), respectively).

In Tables 3 and 4, the Pb and Cu adsorption and desorption efficiency (in mg g^{-1} and %) of biochars Pe350 and Sd350 in solutions containing 100 mg L^{-1} of Pb and Cu, respectively, after a number of cycles using the optimum adsorbent concentration of 5 g L^{-1}, is presented. The % Pb and Cu adsorption efficiency of biochars Pe350 and Sd350 is also presented in Fig. 8(a) and (b), respectively.

From the data presented in Tables 3 and 4 and Fig. 8, it is shown that:

- Pb is adsorbed more efficiently compared to Cu on both biochars.
- The Sd350 biochar shows better adsorption efficiency for both Pb and Cu compared to Pe350 biochar. This conclusion is more noticeable for Cu for which the adsorption efficiency of Sd350 biochar is almost two times higher than that of Pe350 biochar.
- The highest % adsorption of Pb (almost 95 and 97% for Pe350 and Sd350, respectively) and Cu (almost 14 and 35% for Pe350 and Sd350, respectively), is shown in the first cycle, while

thereafter a gradual decrease in the adsorption efficiency is shown.
- Higher % desorption efficiency is shown when 0.1 N HCl is used compared to 0.1 N HNO$_3$.

The adsorption of heavy metals on biochars may be related to the ionic radius of each metal ion studied (1.19 Å for Pb^{2+} and 0.73 Å for Cu^{2+}). Thus, the higher % adsorption is seen for Pb which has larger ionic radius than Cu. The adsorption efficiency of biochars may be also related to the carbon content, while the most probable mechanisms involved are electrostatic attraction and complexation [37–39]. Electrostatic attraction occurs between the biochar surface and Cu^{2+} and Pb^{2+} ions present in solution. On the other hand, surface complexes may be formed on biochars as a result of interactions between heavy metal ions and surface functional groups (e.g. carboxylate, hydroxyl) present in biochars, as also confirmed by FTIR analysis in the present study. Furthermore, it is also mentioned that the presence of surface polar functional groups and the hydrophobic nature of biochars, depends on the molar ratios of O/C and [(O+N)/C] (0.21 and 0.18 for Sd350 and Pe350, respectively, according to the data shown in Table 1).

Table 4
Cu adsorption and desorption efficiency of biochars Pe350 and Sd350

	Cycle 1			Cycle 2	
	Adsorption Cu adsorbed mg g^{-1}	%	Desorption Cu desorbed %	Adsorption Cu adsorbed mg g^{-1}	%
Pe350*	2.7	14	88.9	1.8	9.4
Pe350**	2.6	13.6	80.8	1.4	7.1
Sd350*	6.8	35.2	82.4	6.1	32
Sd350**	6.6	34.8	65.2	5.5	27.8

*Desorption with HCl.
**Desorption with HNO$_3$.
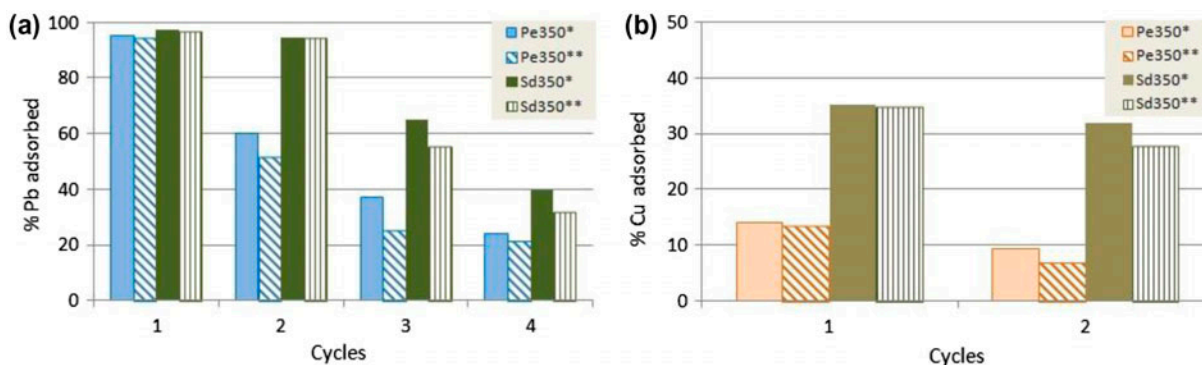
Fig. 8. % Pb and Cu adsorption efficiency ((a) and (b), respectively) of biochars Pe350 and Sd350 in solutions containing 100 mg L^{-1} Pb or Cu (desorption with *HCl or **HNO$_3$).

4. Conclusions

Pecan shells and sawdust may be effectively used for the production of biochar when subjected to slow pyrolysis over a temperature range of 250–550°C. Biochar properties are significantly affected by pyrolysis temperature. Increased temperature results in decreased yield mainly at temperatures higher than 350°C due to condensation of aliphatic compounds, while the char and the volatile matter content increases or decreases, accordingly. DTG confirms the pyrolysis of lignocellulose materials. Aromatic C=O or C=C stretching groups in lignin and other spectra characteristic of cellulosic materials are confirmed by FTIR. The characteristic amorphous peaks of cellulose are shown in XRD patterns of biochars. SEM analysis provides information about the microstructure and porosity of biochar; pore diameter increases when pyrolysis temperature increases from 350 to 550°C.

Biochars produced from pecan shells and sawdust after pyrolysis at 350°C for 60 min, may be used for the removal of heavy metals from solutions. Pb is adsorbed more efficiently compared to Cu on both biochars, while Sd350 biochar shows better adsorption efficiency for both heavy metal ions compared to Pe350 biochar. The most probable metal ion removal mechanisms are electrostatic attraction and complexation as a result of the presence of surface functional groups at the surface of biochars.

Acknowledgments

References

[1] R.S. Kookana, A.K. Sarmah, L. Van Zwieten, E. Krull, B. Singh, Biochar application to soil: Agronomic and environmental benefits and unintended consequences, Adv. Agron. 112 (2011) 103–143.
[2] D.A. Laird, R.C. Brown, J.E. Amonette, J. Lehmann, Review of the pyrolysis platform for coproducing bio-oil and biochar, Biofuels, Bioprod. Biorefin. 3 (2009) 547–562.
[3] J. Manyà, Pyrolysis for biochar purposes: A review to establish current knowledge gaps and research needs, Environ. Sci. Technol. 46 (2012) 7939–7954.
[4] M.P. McHenry, Agricultural bio-char production, renewable energy generation and farm carbon sequestration in Western Australia: Certainty, uncertainty and risk, Agr. Ecosyst. Environ. 129 (2009) 1–7.
[5] W. Ding, X. Dong, I.M. Ime, B. Gao, L.Q. Ma, Pyrolytic temperatures impact lead sorption mechanisms by bagasse biochars, Chemosphere 105 (2014) 68–74.
[6] F. Jia, J. Gan, Comparing black carbon types in sequestering polybrominated diphenyl ethers (PBDEs) in sediments, Environ. Pollut. 184 (2014) 131–137.
[7] T.J. Kinney, C.A. Masiello, B. Dugan, W.C. Hockaday, M.R. Dean, K. Zygourakis, R.T. Barnes, Hydrologic properties of biochars produced at different temperatures, Biomass Bioenergy 41 (2012) 34–43.
[8] B.O. Dias, C.A. Silva, F.S. Higashikawa, A. Roig, M.A. Sanchez-Monedero, Use of biochar as bulking agent for the composting of poultry manure: Effect on organic matter degradation and humification, Bioresour. Technol. 101 (2010) 139–1246.
[9] A. Cabrera, L. Cox, K. Spokas, M.C. Hermosín, J. Cornejo, W.C. Koskinen, Influence of biochar amendments on the sorption–desorption of aminocyclopyrachlor, bentazone and pyraclostrobin pesticides to an agricultural soil, Sci. Total Environ. 470–471 (2014) 438–443.

[10] K.C. Das, M. Garcia-perez, B. Bibens, N. Melear, Slow pyrolysis of poultry litter and pine woody biomass: Impact of chars and bio-oils on microbial growth, J. Environ. Sci. Health., Part A 43 (2008) 714–724.

[11] S. Sohi, E. Lopez-Capel, E. Krull, R. Bol, Biochar, climate change and soil: A review to guide future research, CSIRO Land and Water Science, Report 05/09 (2009).

[12] G. Moussavi, R. Khosravi, Preparation and characterization of a biochar from pistachio hull biomass and its catalytic potential for ozonation of water recalcitrant contaminants, Bioresour. Technol. 119 (2012) 66–71.

[13] E. Agrafioti, D. Kalderis, E. Diamadopoulos, Arsenic and chromium removal from water using biochars derived from rice husk, organic solid wastes and sewage sludge, J. Environ. Manage. 133 (2014) 319–314.

[14] M.J. Antal, M. Grønli, The art, science, and technology of charcoal production, Ind. Eng. Chem. Res. 42 (2003) 1619–1640.

[15] Z. Dai, J. Meng, N. Muhammad, X. Liu, H. Wang, Y. He, P.C. Brookes, J. Xu, The potential feasibility for soil improvement, based on the properties of biochars pyrolyzed from different feedstocks, J. Soil. Sediment. 13 (2013) 989–1000.

[16] R.A. Brown, A.K. Krecher, T.H. Nguyen, D.C. Nagle, W.P. Ball, Production and characterization of synthetic wood chars for use as surrogates for natural sorbents, Org. Geochem. 37 (2006) 321–333.

[17] W.A.W.A.K. Ghani, A. Mohd, G. da Silva, R.T. Bachmann, Y.H. Taufiq-Yap, U. Rashid, A.H. Al-Muhtaseb, Biochar production from waste rubber-wood-sawdust and its potential use in C sequestration: Chemical and physical characterization, Ind. Crops Prod. 44 (2013) 18–24.

[18] J.W. Gaskin, C. Steiner, K. Harris, K.C. Das, B. Bibens, Effect of low-temperature pyrolysis conditions on biochar for agricultural use, T. ASABE. (2008) 2061–2069.

[19] T. Fisher, M. Hajaligol, B. Waymack, D. Kellogg, Pyrolysis behaviour and kinetics of biomass derived materials, J. Anal. Appl. Pyrolysis 62 (2002) 331–349.

[20] C. Ververis, K. Georghiou, N. Christodoulakis, P. Santas, R. Santas, Fiber dimensions, lignin and cellulose content of various plant materials and their suitability for paper production, Ind. Crops Prod. 19 (2004) 245–254.

[21] D. Vamvuka, S. Sfakiotakis, Effects of heating rate and water leaching of perennial energy crops on pyrolysis characteristics and kinetics, Renewable Energy 36 (2011) 2433–2439.

[22] S. Yaman, Pyrolysis of biomass to produce fuels and chemical feedstocks, Energy Convers. Manage. 45 (2004) 651–671.

[23] Z. Liu, A. Quek, S.K. Hoekman, R. Balasubramanian, Production of solid biochar fuel from waste biomass by hydrothermal carbonization, Fuel 103 (2013) 943–949.

[24] D. Angin, S. Şensöz, Effect of pyrolysis temperature on chemical and surface properties of biochar of rapeseed (*Brassica napus* L.), Int. J. Phytorem. 16(7–8) (2014) 684–693.

[25] G. Socrates, Infrared and Raman Characteristic Group Frequencies, third ed., John Wiley, England, 2001.

[26] R.K. Sharma, J.B. Wooten, V.L. Baliga, X. Lin, W. Geoffrey Chan, M.R. Hajaligol, Characterization of chars from pyrolysis of lignin, Fuel 83 (2004) 1469–1482.

[27] X. Cao, W. Harris, Properties of dairy-manure-derived biochar pertinent to its potential use in remediation, Bioresour. Technol. 101 (2010) 5222–5228.

[28] I. Pastorova, R.E. Botto, P.W. Arisz, J.J. Boon, Cellulose char structure: A combined analytical Py-GC-MS, FTIR, and NMR study, Carbohydr. Res. 262 (1994) 27–47.

[29] B. Chen, Z. Chen, S. Lv, A novel magnetic biochar efficiently sorbs organic pollutants and phosphate, Bioresour. Technol. 102 (2011) 716–723.

[30] M. Gray, M.G. Johnson, M.I. Dragila, M. Kleber, Water uptake in biochars: The roles of porosity and hydrophobicity, Biomass Bioenergy 61 (2014) 196–205.

[31] T. Mimmo, P. Panzacchi, M. Baratieria, C.A. Davies, G. Tonon, Effect of pyrolysis temperature on miscanthus (Miscanthus × giganteus) biochar physical, chemical and functional properties, Biomass Bioenergy 62 (2014) 149–157.

[32] A. Caglar, A. Demirbas, Conversion of cotton cocoon shell to liquid products by pyrolysis, Energy Convers. Manage. 41 (2000) 1749–1756.

[33] X. Cao, L. Zhong, X. Peng, S. Sun, S. Li, S. Liu, R. Sun, Comparative study of the pyrolysis of lignocellulose and its major components: Characterization and overall distribution of their biochars and volatiles, Bioresour. Technol. 155 (2014) 21–27.

[34] M. Catinon, S. Ayrault, L. Spadini, O. Boudouma, J. Asta, M. Tissut, P. Ravanel, Tree bark suber-included particles: A long-term accumulation site for elements of atmospheric origin, Atmos. Environ. 45(5) (2011) 1102–1109.

[35] D. Houben, P. Sonnet, J.-T. Cornelis, Biochar from Miscanthus: A potential silicon fertilizer, Plant Soil 374 (2014) 871–882.

[36] L.E. Hernandez-Mena, A.A.B. Pécora, A.L. Beraldo, Slow pyrolysis of bamboo biomass: Analysis of biochar properties, Chem. Eng. Trans. 37 (2014) 115–120.

[37] X.-J. Tong, J.-Y. Li, J.-H. Yuan, R.-K. Xu, Adsorption of Cu(II) by biochars generated from three crop straws, Chem. Eng. J. 172(2–3) (2011) 828–834.

[38] A.W. Samsuri, F. Sadegh-Zadeh, B.J. Seh-Bardan, Adsorption of As(III) and As(V) by Fe coated biochars and biochars produced from empty fruit bunch and rice husk, J. Environ. Chem. Eng. 1 (2013) 981–988.

[39] X. Xu, X. Cao, L. Zhao, Comparison of rice husk- and dairy manure- derived biochars for simultaneously removing heavy metals from aqueous solutions: Role of mineral components in biochars, Chemosphere 92 (2013) 955–961.